PHILOSOPHICAL TRANSACTIONS B

royalsocietypublishing.org/journal/rstb

Research

Cite this article: McKnight JC *et al*. 2021 When the human brain goes diving: using near-infrared spectroscopy to measure cerebral and systemic cardiovascular responses to deep, breath-hold diving in elite freedivers. *Phil. Trans. R. Soc. B* **376**: 20200349. https://doi.org/10.1098/rstb.2020.0349

Accepted: 4 March 2021

One contribution of 10 to a theme issue 'Measuring physiology in free-living animals (Part II)'.

Subject Areas:
physiology

Keywords:
near-infrared spectroscopy, freediving, breath-hold diving, SpO_2, cererbal oxygenation, diving physiology

Author for correspondence:
J. Chris McKnight
e-mail: jcm20@st-andrews.ac.uk

Electronic supplementary material is available online at https://doi.org/10.6084/m9.figshare.c.5429435.

THE ROYAL SOCIETY PUBLISHING

When the human brain goes diving: using near-infrared spectroscopy to measure cerebral and systemic cardiovascular responses to deep, breath-hold diving in elite freedivers

J. Chris McKnight[1,3], Eric Mulder[3], Alexander Ruesch[5], Jana M. Kainerstorfer[5,8], Jingyi Wu[5], Naser Hakimi[6], Steve Balfour[2], Mathijs Bronkhorst[6], Jörn M. Horschig[6], Frank Pernett[3], Katsufumi Sato[7], Gordon D. Hastie[1], Peter Tyack[1] and Erika Schagatay[3,4]

[1]Sea Mammal Research Unit, Scottish Oceans Institute, and [2]Sea Mammal Research Unit Instrumentation Group, Scottish Oceans Institute, University of St Andrews, St Andrews, UK
[3]Department of Health Sciences, and [4]Swedish Winter Sport Research Center (SWSRC), Mid Sweden University, Östersund, Sweden
[5]Department of Biomedical Engineering, Carnegie Mellon University, 5000 Forbes Avenue, Pittsburgh, PA 15213, USA
[6]Artinis Medical Systems BV, Einsteinweg 17, 6662 PW Elst, The Netherlands
[7]Atmosphere and Ocean Research Institute, The University of Tokyo, 5-1-5 Kashiwanoha, Kashiwa, Chiba 277-8564, Japan
[8]Neuroscience Institute, Carnegie Mellon University, 4400 Forbes Ave., Pittsburgh, PA 15213, USA

JCM, 0000-0002-3872-4886; MB, 0000-0002-0410-0303; JMH, 0000-0002-0159-431X; FP, 0000-0002-9787-6660; GDH, 0000-0002-9773-2755; PT, 0000-0002-8409-4790

Continuous measurements of haemodynamic and oxygenation changes in free living animals remain elusive. However, developments in biomedical technologies may help to fill this knowledge gap. One such technology is continuous-wave near-infrared spectroscopy (CW-NIRS)—a wearable and non-invasive optical technology. Here, we develop a marinized CW-NIRS system and deploy it on elite competition freedivers to test its capacity to function during deep freediving to 107 m depth. We use the oxyhaemoglobin and deoxyhaemoglobin concentration changes measured with CW-NIRS to monitor cerebral haemodynamic changes and oxygenation, arterial saturation and heart rate. Furthermore, using concentration changes in oxyhaemoglobin engendered by cardiac pulsation, we demonstrate the ability to conduct additional feature exploration of cardiac-dependent haemodynamic changes. Freedivers showed cerebral haemodynamic changes characteristic of apnoeic diving, while some divers also showed considerable elevations in venous blood volumes close to the end of diving. Some freedivers also showed pronounced arterial deoxygenation, the most extreme of which resulted in an arterial saturation of 25%. Freedivers also displayed heart rate changes that were comparable to diving mammals both in magnitude and patterns of change. Finally, changes in cardiac waveform associated with heart rates less than 40 bpm were associated with changes indicative of a reduction in vascular compliance. The success here of CW-NIRS to non-invasively measure a suite of physiological phenomenon in a deep-diving mammal highlights its efficacy as a future physiological monitoring tool for human freedivers as well as free living animals.

This article is part of the theme issue 'Measuring physiology in free-living animals (Part II)'.

1. Introduction

Central to the capacity for repeated or prolonged breath-hold diving in animals, such as seals and humans, is the suite of cardiovascular responses, collectively

© 2021 The Author(s) Published by the Royal Society. All rights reserved.

termed the 'diving response', that serve to conserve oxygen by downregulating its rate of consumption [1,2]. Upon submersion, diving mammals respond with a significant redistribution of blood achieved through peripheral arterial constriction, preferentially distributing most of the cardiac output to high-priority tissues such as the brain, heart, adrenals and splanchnic organs [3,4]. The consequent increase in peripheral resistance is compensated for by a simultaneous and significant reduction in heart rate, moderately reduced stroke volume and reduced myocardial contractility; matching left ventricular output to the restricted vascular beds and decreased venous return [4,5]. Although these cardiovascular adjustments to diving reduce the rate of blood oxygen depletion, extending aerobic dive duration for diving animals [6], promoting efficient foraging and prolonging apnoea duration in humans [7], up to now their study has been mainly limited to measurements in the laboratory. Human underwater foragers successfully freedive repeatedly to 20 m for hours daily with dive durations under 1 min [7], and competition freedivers can perform static breath-holds lasting over 10 min, swim 300 m underwater and—perhaps most remarkably—reach depths in excess of 100 m during swimming dives lasting over 4 min (www.aidainternational.org). Sharing many physiological features with consummate diving mammals [7], these human deep freedivers can potentially serve as a tractable generalized model for work on diving mammals.

Despite extensive knowledge on the mechanistic drivers and moderating factors of the diving response [3], how the fundamental components of the response, such as tissue-specific perfusion and oxygenation, vary across tissues between dives and species during free-ranging diving, and its impact on blood gas tensions and gas management is limited. Much of our understanding of arterial or venous blood oxygenation in diving animals, including humans, is based on haematological variables from the major vasculature using implanted intravascular oxygen sensors [8,9], or cross-sectional measurements [6,10,11]. Information at the level of individual tissues, including haemodynamics and oxygenation changes, is even more limited and predominately derived from cross-sectional measurements from lethally sampled animals after forced dives [5,12], numerical modelling exercises [13] or simulated, controlled diving experiments [14]. These data, and methods of data collection, have provided a vitally important basis for our understanding of the haemodynamic and gas tension changes engendered by breath-hold diving. However, continuous measurements of parameters of haemodynamic changes and blood oxygenation remain elusive—particularly in deep-diving animals [15,16]. Developing a greater capacity for continuous oxygenation and haemodynamic measurement is important both for research, such as understanding potential vulnerabilities and consequences of observed physiological responses to anthropogenic disturbance on diving animals [17], and for applied science, such as improving safety in human breath-hold diving [18]. Advances in wearable biomedical equipment, such as continuous-wave near-infrared spectroscopy (CW-NIRS), may provide a critical tool in reducing this knowledge gap.

CW-NIRS is a non-invasive, optical-based technology that measures relative concentration changes in oxyhaemoglobin [ΔO_2Hb], and deoxyhaemoglobin [ΔHHb] [19]. Changes in [ΔO_2Hb] and [ΔHHb] can provide high-resolution measurements of relative blood volume changes [20], mixed arterial–venous tissue-specific haemoglobin oxygen saturation (tissue saturation index (TSI)) [21], arterial oxygen saturation (SpO_2) [22], as well as heart rate and information on cardiac waveform (similar to photoplethysmography [23]).

Here, we describe the application of a custom-developed spatially resolved CW-NIRS tag designed to function on deep-diving humans which provide a useful diving model for a test of CW-NIRS as a technology for physiological measurement in diving animals. We monitored changes in cerebral blood volume (CBV), cerebral TSI, SpO_2, heart rate and diving behaviour in elite freedivers, deep-diving of their own volition at sea. Studying diving humans, we highlight the capacity of CW-NIRS to collect a variety of high-resolution cardiovascular and cerebrovascular data during deep dives and present these data, with some comparisons to diving mammals, to demonstrate the use of CW-NIRS both to understand human freediving physiology and as a comparative diving physiology research tool that could assist in improving our physiological understanding of animal ecophysiology.

2. Methods

(a) Near-infrared spectroscopy system

An archival NIRS sensor, PortaDiver, was developed from an existing wearable dual-wavelength CW-NIRS system for humans (PortaLite mini) that simultaneously uses the modified Beer–Lambert Law [24] and spatially resolved spectroscopy methods. Changes in the concentration of [ΔO_2Hb] and [ΔHHb] can be calculated from changes in light absorption using the modified Beer–Lambert Law, which describes optical absorption changes in a scattering medium. Because the absolute chromophore concentration is unknown, relative values for [O_2Hb] and [HHb] were measured as a change from the start of each dive in micromolar units per litre of tissue ($\mu mol\ l^{-1}$). This allowed calculation of total Hb ([ΔHbT] = [O_2Hb] + [ΔHHb]) that can be used as a proxy for changes in blood volume. TSI is a measure of tissue oxygen saturation of haemoglobin (combined arterial and venous contribution, measured using a modified diffusion equation and validated both *in vitro* and *in vivo* [25]) and uses multiple channels to remove the contribution of non-cerebral tissue from the measurement [26]. A quality control factor (QCF) which estimates model fit was used to ensure TSI reliability. The QCF is a correlation factor to indicate the quality of the measured slope, where the value 1 is a perfect fit and 0 is no fit. TSI values with a QCF value lower than 99.9 were removed from the dataset as these values are a result of insufficient contact between emitters and/or receivers with skin.

NIRS measures a volume of tissue containing microvasculature, comprising capillary, arteriolar and venular beds but not large arteries and veins. The PortaLite mini consisted of a sensor body, housed in an aluminium case with a removable O-ring sealed lid (with three optical acrylic windows), and a sensor head. To waterproof the sensor head, the light emitting diodes (LEDs), photodiode receiver and printed circuit boards (PCBs) of the sensor head were first fitted into optically opaque polyoxymethylene housings. The housings were filled with spectrally transparent epoxy (EPO-TEK 301, Epoxy Technology, Billerica, MA, USA). To ensure that epoxy encapsulated the electronics but did not cover the optical window on the optodes, the sensor head was cradled in a custom-built silicone mould. This allowed the internal components to be filled and waterproofed by epoxy but ensured the external surface and

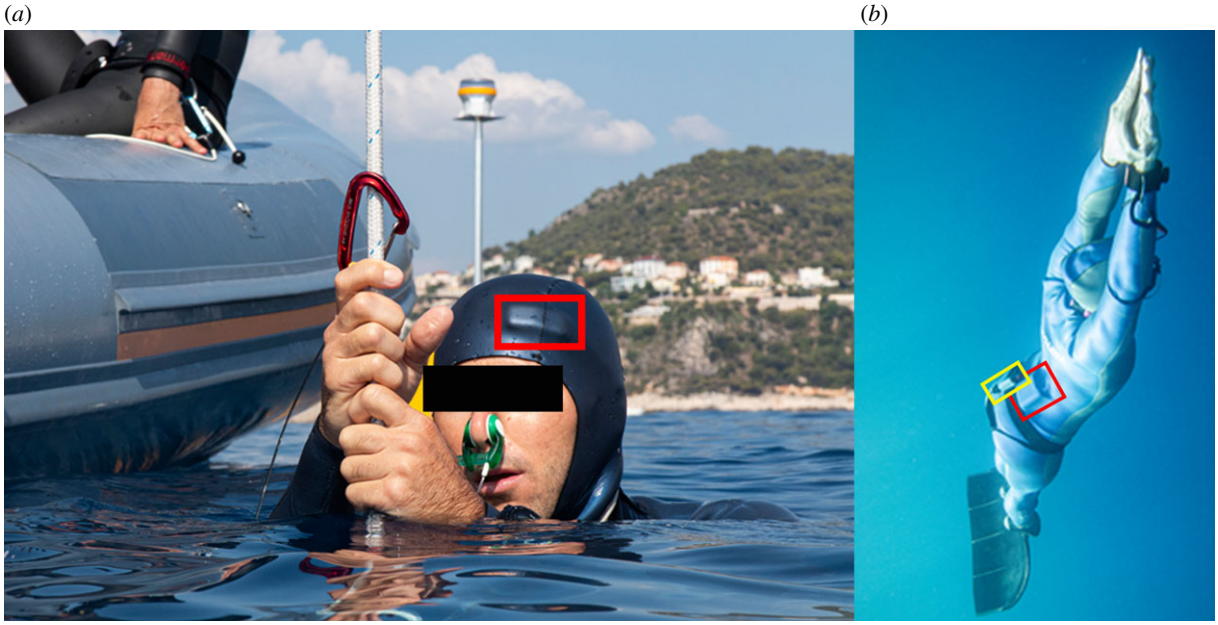

Figure 1. Monitoring diving physiology and behaviour in elite freedivers. (*a*) Location of NIRS sensor head over the pre-frontal cortex (red box). (*b*) Respective placements of NIRS sensor body (red box, right) and Little Leonardo W1000-PD3GT (yellow box, left). (Online version in colour.)

LEDs remained exposed. Once the housings were filled with epoxy, an optically opaque lid was placed onto the housing and fixed with two screws. Finally, the exterior of the housings and interoptode were potted in optically transparent polyurethane for flexibility, allowing the sensor head to conform to the shape of each divers head. The distance between light sources and detector were 30 mm (850 nm and 751 nm optode), 35 mm (852 nm and 751 nm optode) and 40 mm (851 nm and 752 nm optode), allowing optical penetration to three different tissue depths (larger spacing between the optode and receiver allows deeper optical penetration). The response time of the PortaDiver was less than or equal to 0.1 s. The PortaDiver was controlled via a combination of magnetic reed switches and Bluetooth, allowing the system to be controlled from within the waterproof housing without the necessity for opening. Following marinization of the instrument, the device was returned to the manufacturer (Artinis Medical Systems BV) for calibration, testing and approval of accurate functionality. The PortaDiver measured [ΔO_2Hb], [ΔHHb] concentration changes and cerebral blood oxygen saturation index (TSI—expressed as a percentage). The NIRS data were used to calculate changes in total haemoglobin (Δ[HbT] = [ΔO_2Hb] + [ΔHHb]), SpO_2 and heart rate.

Swimming movements were measured with a Little Leonardo W1000-PD3GT (Little Leonardo, Tokyo, Japan), (electronic supplementary material, figure S1A) which logged tri-axial acceleration (32 Hz), depth (1 Hz) and temperature (1 Hz) (figure 1).

(b) Human diving trials

Five elite male competition freedivers, all active competitors, volunteered to participate during training dives. The PortaDiver and Little Leonardo W1000-PD3GT bio-logging devices were attached to a diver while onboard a boat before each recording session. The PortaDiver sensor body was placed inside the diver's wetsuit. The PortaDiver sensor head was inserted into the diver's wetsuit hood above the left eye, on the forehead over the pre-frontal cortex (figure 1). The Little Leonardo was clipped to the diver's weight belt (figure 1) with low strength cable ties to ensure it would come away from the freedivers if the instrument became tangled. Divers were then operating of their own volition throughout their freediving training session. Safety divers were present during all dives. All divers used 'lung packing' (glossopharyngeal insufflation) to fill lungs above normal total lung capacity before the start of each dive [27]. Dives were made during three depth competition disciplines: constant weight vertical swimming to depth using fins or a monofin (eight dives), constant weight swimming without fins (four dives) and free immersion (five dives) involving the diver manually pulling down and up on a rope using their arms (see Schagatay [7] for details). Once the divers had completed their training session and exited the water, the instruments were removed. Scientific procedures involving freedivers complied with the Helsinki agreement and were approved by the Regional Committee for Medical and Health Research Ethics (Dnr 2019-05147).

(c) Seal near-infrared spectroscopy data

To demonstrate the translatable capacity of NIRS from humans to diving animals, NIRS data, collected from a juvenile grey seal (*Halichoerus grypus*), were also included in the cardiac waveform analysis described below. Seal data were collected using a wearable NIRS device ('Brite24' Artinis Medical Systems BV, Einsteinweg, The Netherlands) with 16 dual-wavelength emitters and eight photodiode detectors, configured to provide 28 channels. The LED emitters each had two NIR light sources with wavelengths of 755–758 and 839–854 nm and the eight photodiode detectors had an incorporated ambient light filter. The optode–detector trace visualised had a separation distance of approximately 30 mm (long channels). Data were collected on a juvenile grey seal anaesthetized using a combination of midazolam (Hypnovel, Roche Products Ltd, UK; 5 mg ml^{-1} solution, 0.03 ml kg^{-1} IM as a premedication sedative and 0.01 ml kg^{-1} IV to control tremors) and ketamine (Ketaset, Zoetis, UK 100 mg ml^{-1} solution, 0.01 ml kg^{-1} IV). Procedures for capture, handling and housing of animals conformed to the Animals (Scientific Procedures) Act 1986, under the Sea Mammal Research Unit's Home Office licence (no. 70/7806) and were performed by personnel deemed competent under EU directive of the protection of animals used for scientific purposes.

(d) Heart rate extraction

A heart rate derivation algorithm presented in [28] was applied to extract heart rate from the NIRS signal. The algorithm consists

of three steps: (i) pre-processing, (ii) heart rate extraction, and (iii) heart rate correction. In the pre-processing step, a 100th-order zero-phase bandpass finite impulse response filter between 0.1 and 4 Hz was applied. This effectively reduces the influence of motion and systemic artefacts in the data and allows for more reliable heartbeat detection.

In the heart rate extraction step, the peak points in the pre-processed signal were detected by applying the AMPD method [29]. AMPD is an automatic peak detection algorithm applicable to noisy periodic and quasi-periodic signals. It is based on calculating and analysing the local maxima scalogram which produces a matrix comprising the scale-dependent occurrences of the local maxima. After applying the AMPD peak detection algorithm, the momentary heart rate is obtained by calculating the peak-to-peak time interval. The continuous heart rate signal is then constructed through cubic interpolation.

In the heart rate correction step, a windowing approach based on the method presented in [28] is used to reduce errors due to false alarms of peak detection. In this method, a permissible range is initially defined for each extracted heart rate value. The permissible range is distributed around the mean of the extracted heart rate of the previous 4 s (m) with a permissible deviation. The permissible deviation is created by a weighted ($k = 21$) ratio of the total standard deviation of the heart rate signal from the start to the present time (SD) to the standard deviation of the previous 4 s (s.d.). Extracted heart rates which fall outside of the permissible range ($m - k \times \mathrm{SD/s.d.} < \mathrm{HR} < m + k \times \mathrm{SD/s.d.}$) are removed and the samples are interpolated using a cubic spline.

(e) Arterial oxygen saturation extraction

Cardiac-related pulsatile signals can be detected in different parts of the human body, including the finger, ear lobe and forehead by using NIRS monitoring. These pulsatile signals occur as a result of attenuation of light by the increase in arterial blood volume during systole in the cardiac cycle [30]. Consequently, the detected oscillations in the optical signal can be attributed to the arterial blood, with a saturation which is then related to the oscillatory components of the optical densities at two or more wavelengths. Pulse oximetry exploits these pulsatile signals to calculate SpO_2. We exploit this same principle here to calculate SpO_2 using NIRS [22,30,31]. Specifically, we employ the SpO_2 extraction methodology, validated against pulse oximetry measures of SpO_2, used by Menssen *et al*. [22]. SpO_2 extraction was performed in MATLAB (The MathWorks Inc., Natick, MA, USA), and the algorithm consisted of three steps: (i) pre-processing, (ii) frequency spectrogram generation, and (iii) SpO_2 calculation. In the pre-processing step, a third-order zero-phase Butterworth filter at 0.4 Hz was applied to the measured [ΔO_2Hb] and [ΔHHb] traces. Spectrograms of the filtered [ΔO_2Hb] and [ΔHHb] were generated, from which heart rate variation over time can be observed. At a particular time point in the spectrogram, heart rate was identified by the peak frequency component and the spectral power of [ΔO_2Hb] and [ΔHHb] at the frequency was extracted. SpO_2 was calculated using these values at each time point such that $SpO_2 = [\Delta O_2\text{HbHR}]/[\Delta O_2\text{HbHR} + \Delta\text{HHbHR}]$. The extraction of SpO_2 requires the calculation of fast Fourier transforms (FFTs) in defined time bins, creating a spectrogram. The time bin size determines the resolution of the FFT and, therefore, the precision of the extraction of spectral power at the heart rate, which is the fundamental information for SpO_2 calculations. Typically, bin size of 10–35 s was used (mean = 26.3 s) over which one FFT was calculated and from which one SpO_2 value could be extracted. Because the SpO_2 value was assigned to the centre time point of the time bin, no SpO_2 values could be calculated prior to half the bin size from the start and the end of the measurement.

(f) Cardiac waveform analysis by pulse averaging in freedivers

To investigate potential changes in cardiac waveform and changes in heart rate associated with diving, and potentially indicative of changes in blood pressure and/or change in vascular compliance, analysis of the pulse shape across cardiac cycles was analysed with particular attention focused on three waveform features: (i) percussive wave (originating from the contraction of the left ventricle and ejection of blood); (ii) tidal wave (caused by the elasticity of the aortic wall); and (iii) diastolic minimum (caused by full relaxation of the heart). Signal processing was performed using MATLAB. Raw light intensities were extracted, and the modified Beer–Lamberts Law was applied [24]. This allowed the computation of zero-centred [ΔO_2Hb] and [ΔHHb] for every given source–detector combination; [ΔHbT] was calculated as the sum of [ΔO_2Hb] and [ΔHHb]. Signals were visually inspected for movement artefacts, which were removed from the data. A high-pass filter with a transition band of 0.1–0.2 Hz was used to remove baseline drifts.

The data were upsampled from 10 to 100 Hz sampling frequency. The peak finding algorithm was then applied to the first derivative of the [ΔHbT], as this proved to be more robust than a direct peak finding of the diastolic valley. The search parameters were similar to those described above for the seal, with a weighting factor of 0.5 for the minimum peak prominence and a minimum peak distance of 0.7 s. A time window between 0.5 s before and 2.9 s after the onset of every detected pulse was extracted and a moving average was applied. Fifteen consecutive pulses were averaged, to improve signal to noise ratios. Outliers were removed by z-score rejection. To identify the true diastolic minima, we first searched for all local minima in every cardiac pulse using the 'islocalmin' function ('islocalmin', MATLAB). For every local minimum in the starting pulse, a tracking algorithm over time was implemented across all following pulses. The tracking was a search for the closest local minimum when compared with the previous pulse, with respect to the position in time in which the local minimum occurred (T_{relative}), the difference in height (H) and prominence (P) of the minimum as well as the distance in time to the first, original, diastolic minimum (T_{origin}). The search radius between 0.5 s before and 1 s after the previous local minimum was chosen. Peak heights and prominences were normalized to the systolic maximum of every pulse, making it a systolic peak height percentage. Time measurements were normalized to be a percentage of the total time of 2.9 s following the original diastolic valley. The best successor to the current local minimum was determined by the minimum of the error function, $\mathrm{EF} = T_{\mathrm{relative}} + 2\ T_{\mathrm{origin}} + H - P$. Once the tracking of all local minima was complete, the algorithm was repeated starting from the last pulse going backwards to the first pulse. Finally, the most probable trace of local minima was determined to be the second diastolic valley in the signal by comparing goodness of fit function defined as $\mathrm{GOF} = \bar{P} - \bar{H} - 1.5\,\overline{T_{\mathrm{origin}}}$, with $\bar{P}$ as the average prominence in the trace, $\bar{H}$ is the average valley height and $\overline{T_{\mathrm{origin}}}$ the average time passed since the pulse onset. Waveforms were normalized in height and length to observe the pulse shape change independent of the change in heart rate and pulse height. The average diving depth and average heart rate for every pulse was determined. Pulses were then averaged in bins of 5 m diving depth or 10 bpm of heart rate, respectively.

(g) Cardiac waveform analysis by pulse averaging in the seal

An elliptical high-pass filter with a transition band between 0.2 and 0.3 Hz was created ('ellip', MATLAB) and applied to the data through the phase preserving function 'filtfilt' ('filtfilt',

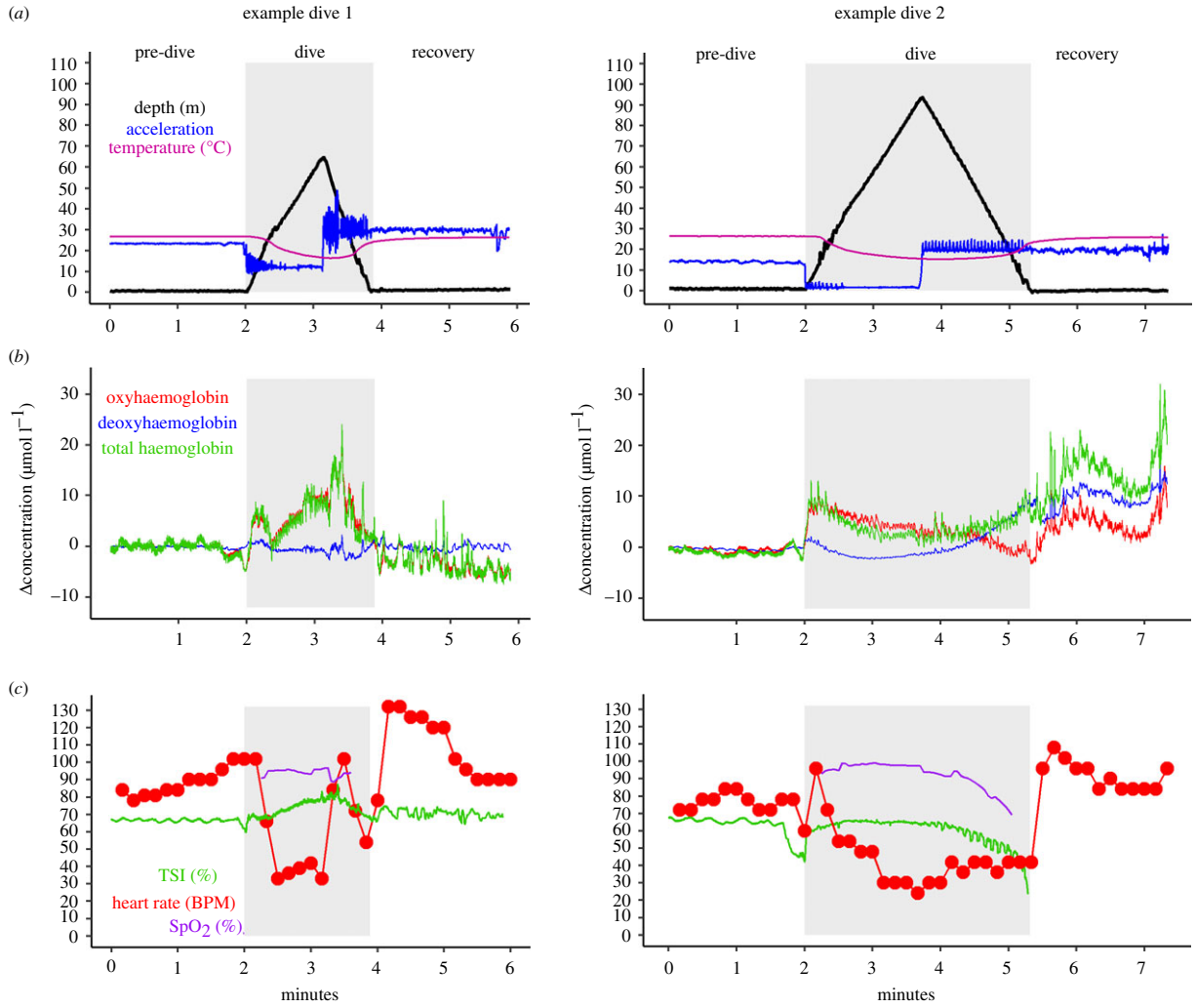

Figure 2. Monitoring physiological variables in freedivers. Two example dives to 67 and 97 m from two freedivers, showing (*a*) dive and temperature data and (*b*) cerebral haemodynamic responses. (*c*) Heart rate, cerebral and arterial blood oxygen responses. High-frequency peaks and troughs in the accelerometry signal are indicative of leg movements associated with swimming in the CWT dive in example 1 and arm movements of pulling along the rope in an FIM dive in example 2. During early descent, the divers swim intensely to overcome positive buoyancy which is seen as high-amplitude peaks on the acceleration trace, while later during the descent, the negatively buoyant divers free fall. At the bottom of the dive, when the divers turn and swim upwards against negative buoyancy, the acceleration trace, again, shows high-amplitude peaks throughout ascent. Oscillations in TSI from minutes 4–5 in example 2 were probably the result of involuntary breathing movements [14]. TSI measurement in example 2 was lost on surfacing as one of three NIRS channels lost contact with the diver's head.

MATLAB). The data were then upsampled from 10 to 100 Hz using spline interpolation. In combination with a pulse averaging described below, this procedure allowed certain details from the cardiac pulsation beyond the low sampling frequency of 10 Hz to be retained.

A direct peak finding approach on the inverted [ΔHbT] signal was then performed using the 'findpeaks' function ('findpeaks', MATLAB) to determine diastolic minima in the signal. Search parameters included a minimum peak prominence of 1 s.d. of the signal, divided by the square root of the upsampling ratio of 10, weighted by an empirically determined factor of 0.2. The minimal peak distance was determined to be 0.5 s and the minimum peak height was set to 0. A time window between 0.5 s before and 2.9 s after, the found diastolic minimum was extracted. A moving average across five consecutive pulses was then applied. To remove outliers caused by motion artefacts or failed diastolic minima extraction, a *z*-score rejection across the pulses for every individual point in time was applied. If at any given time a $z > 3$ was determined, the entire pulse was rejected. Figure 4*b* shows these averaged curves, zeroed to the first diastolic minimum and cut off after the second diastolic minimum found in each individual averaged pulse.

3. Results

Data were successfully collected from each of the 17 dives made by the freedivers. Dives ranged in duration from 49 to 249 s (mean = 130 s; s.d. = ±64 s) and ranged in depth from 21 to 107 m (mean = 50 m; s.d. = ±26 m). All dives generated continuous data, which could be analysed, while some loss of data occurred in the seconds immediately before the divers surfaced. Insufficient contact between one NIRS channel and the skin of the freedivers meant TSI could not be caluculated for four dives (electronic supplementary material, table S1). Diving profiles, cerebral haemodynamic responses, heart rate, cerebral and arterial blood oxygen responses and temperature data are shown for two example dives, one constant weight to 67 m and one free immersion dive to 97 m, in figure 2.

(a) Cortical haemodynamic responses

Continuous measurements of [ΔO_2Hb] and [ΔHHb] allowed the continuous changes in CBV, cerebral TSI and SpO_2 to be

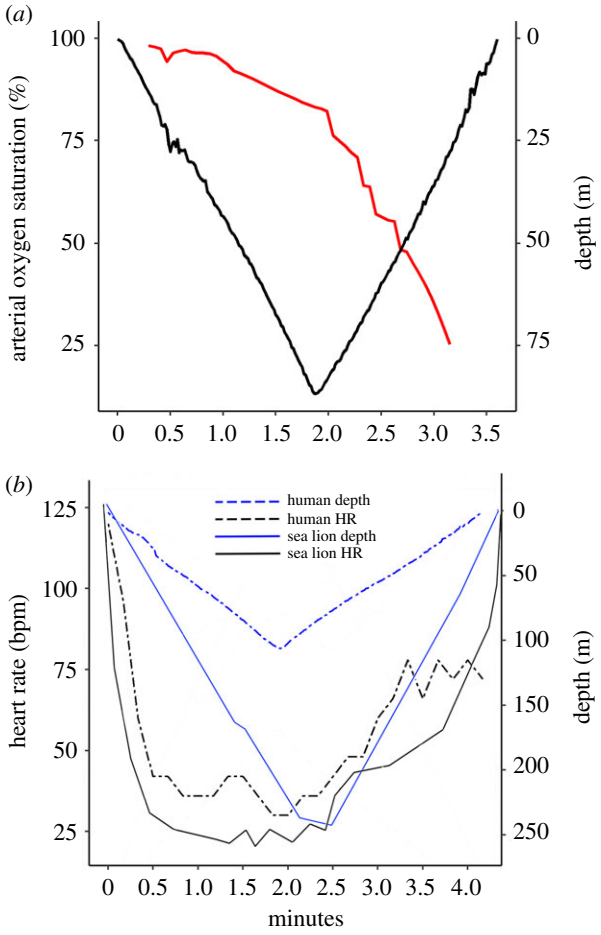

Figure 3. (*a*) Arterial oxygen saturation (SpO_2—red line) and depth data from a dive resulting in the lowest arterial blood oxygenation recorded (25%). (*b*) Heart rate and depth profiles for a human diver (80 kg) perform the deepest dive recorded (107 m) and an 81 kg California sea lion (*Zalophus californianus*) diving to 240 m (data re-drawn with permission from McDonald & Ponganis [32]). (Online version in colour.)

calculated for all 17 dives. [ΔO_2Hb] and [ΔHHb] showed little change during pre-diving except for slow-wave oscillations while divers were still breathing. However, immediately before diving, when divers performed 'lung packing', there was a reduction in [ΔO_2Hb] with a consequent fall in CBV and TSI (as visible before the onset of diving in figure 2). Upon diving [ΔO_2Hb] rose to exceed pre-diving levels, with a consequent elevation in CBV above pre-diving levels and restoration of TSI to pre-lung packing levels (figure 2).

Across the remainder of the diving period, patterns of change in [ΔO_2Hb] and [ΔHHb] varied across dives and divers, which could be expected with different individuals performing dives of differing depths, durations and disciplines. As demonstrated in figure 2*b*, two dives from different divers show considerable differences in patterns of change in [ΔO_2Hb], [ΔHHb] and [ΔHbT] over the diving period. In example dive 1, cerebral haemodynamic changes resulted in TSI remaining close or above pre-diving levels throughout the dive. However, in example dive 2, while TSI remained high throughout the descent phase of the dive, it declined during ascent and showed a marked increase in the rate of decline during the last 10–15 m as [ΔHHb] and CBV rose. This phenomenon of low TSI, concomitant with increased CBV engendered by rising [ΔHHb], was seen in 8 of the 17 dives logged—all of which were the longest dives performed by participants.

SpO_2 dynamics were similar across all dives. SpO_2 remained close to pre-diving levels (greater than 95%) during descent, before generally declining during ascent. Greater declines in SpO_2 were observed during longer dives, with the lowest SpO_2 value recorded being 25% (figure 3*a*). On longer dives, SpO_2 declines were generally concomitant with declines in TSI, except for the previously described rapid drops in TSI in the last 10–15 m of ascent.

(b) Cardiac responses

Blood volume changes associated with cardiac pulsation (as measured here in the brain and scalp of the freedivers), evident in the [ΔO_2Hb] signal (figure 4) and to a lesser extent in the [HHb] signal, allowed heart rate to be extracted for each of the 17 dives. Heart rate changes across the period of diving showed a similar pattern across all dives. Following the onset of diving, heart rate declined during the dive descent (figures 2*c* and 3*b*). Minimum heart rate was reached at the bottom of the dive after a period of passive descent during 'free fall', before showing an overall increase during ascent, especially during early ascent involving exercise to overcome negative buoyancy (figures 2*c* and 3*a*).

The magnitude of reduction in heart rate across the descent phase of each dive was pronounced and, in some cases, comparable in magnitude to diving mammals (figure 3*b*). As shown in figure 4*b* (red line), where a diver exhibits less than 27 beats over 60 s, sustained low heart rates were not uncommon. Indeed, the longest interbeat interval measured in the current study was 5.4 s (figure 4*c*), representing a heart rate of 11 bpm. The high-quality cardiac pulsation signal within the data allowed participants' cardiac waveforms to be analysed for potential changes associated with diving. By performing cardiac waveform analysis on the cardiac pulsation signal, it was apparent that in 9 of 17 dives, divers' cardiac waveforms showed progressive changes with heart rate and depth—specifically, the height of the percussive peak (pulse magnitude) and the prominence of the tidal peak both increased (figure 5*a*) at lower heart rates. Similar signal analysis for heart rate extraction and cardiac waveform channel was performed on the seal data to validate the transferability of the NIRS signal and signal processing to marine mammals (figure 5*b*). Similar to human data, at lower heart rates, the example seal data showed increased percussive peak height (pulse magnitude) (figure 5*c*) and greater prominence of the tidal peak (figure 5*a*,*b*). Figure 5*d*,*e* shows participant waveforms normalized in height and length, therefore independent of changes in heart rate, demonstrating that with both increased depth and lowered heart rate (which themselves are correlated; figures 2 and 3*b*), there was greater prominence in the tidal peak.

4. Discussion

The results presented here demonstrate the capacity of non-invasive CW-NIRS to function as a physiological monitoring tool in trained human freedivers during diving to extreme depth. Extremely low values for both heart rate and SpO_2 were recorded in these dives, as well as variable cerebral haemodynamic pattern, and transient changes in cardiac

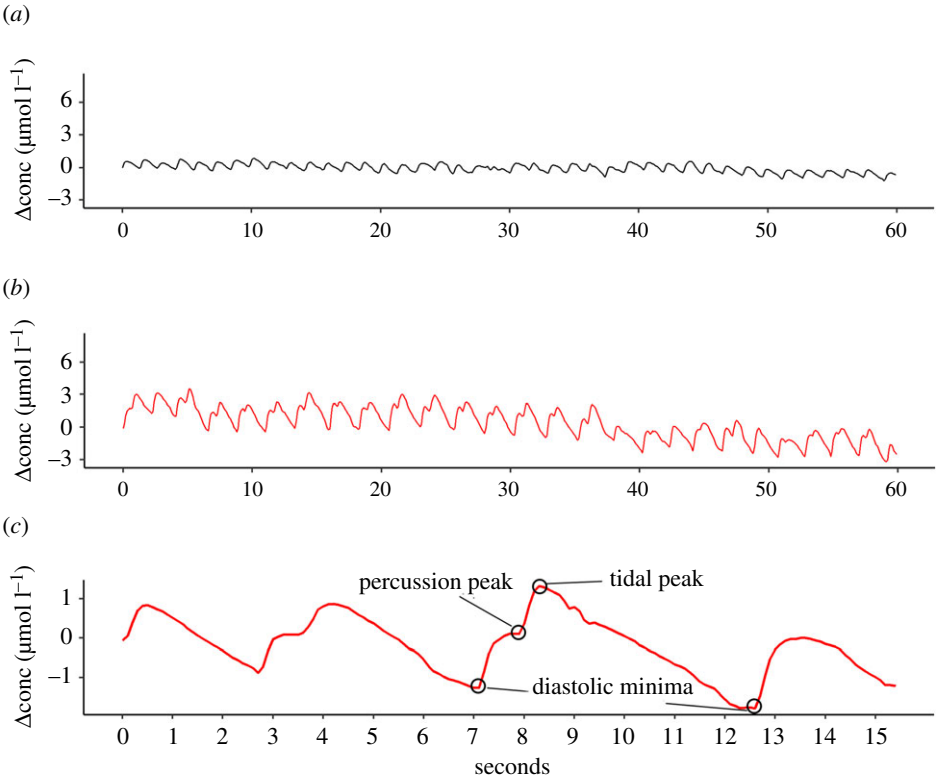

Figure 4. Raw [O_2Hb] traces visualizing heart rate and cardiac waveform. (*a*) Shape and magnitude of a normal cardiac waveform at 41 bpm. (*b*) Cardiac waveform with increased magnitude and pronounced tidal waves at a heart rate of 27 bpm. (*c*) Cardiac waveforms across four cardiac cycles with three key features identified—(i) percussive wave (originating from the contraction of the left ventricle and ejection of blood); (ii) tidal wave (caused by the elasticity of aortic wall); and (iii) diastolic minimum (caused by relaxation of the heart)—showing the transient changes in cardiac waveform on the longest interbeat interval (5.4 s) recorded. (Online version in colour.)

waveform in some divers. The capacity to simultaneously measure haemodynamic changes, and calculate tissue-specific and arterial oxygenation, along with heart rate and cardiac waveform changes, show that CW-NIRS has the potential to provide continuous high-resolution physiological changes in naturalistic conditions for humans as well as other diving animals.

(a) Cortical haemodynamic responses

Continuous measurements of tissue-specific haemodynamic changes in diving animals remain elusive. However, the NIRS instrument in the current study successfully provided continuous measurements of CBV and tissue-oxygenation, and suggests that NIRS could facilitate in addressing this knowledge gap. Indeed, little is known about patterns of change in tissues, such as the brain, in diving animals [4,12,20]; with no information on context specific-changes (i.e. deep high-exertion foraging dives versus shallow transiting dives) as measurements have been restricted to predictable simulated foraging [20] or simulated diving [4,12] paradigms. Importantly, in the current study, it was clear that different divers, dive depths, diving disciplines and respiratory mechanics affected patterns of change in CBV and TSI. Nevertheless, it is unknown whether such variability in diving CBV and TSI exists in other diving mammals, how this could be affected by activity, nor how this may vary between species. Even initial deployments of NIRS on vertically diving animals could provide interesting new insights into cerebral haemodynamic and oxygenation changes.

In the current study, two phases of diving resulted in TSI deflections in the freedivers. Firstly, during pre-diving lung packing, and secondly, in the second half of long and deep dives. TSI deflections during lung packing were driven by a reduction in [ΔO_2Hb] and CBV (figure 2*b*). This may be the result of a reduction in cerebral blood flow through reduced arterial blood pressure and cardiac output associated with the lung packing manoeuvre [33]. Reduced TSI in the second half of longer and deeper dives resulted in marked reductions in end-dive cerebral TSI values. Low end-dive TSI may not simply be a function of longer breath-holds, as the rapid decline in TSI at the end of the dive was a function of increased cortical [ΔHHb] but not declining [ΔO_2Hb] (figure 2, example dive 2). Thus, elevated [ΔHHb] and CBV does not appear to solely be a product of diminishing SpO_2, but also, potentially, hypercapnia affecting haemoglobin oxygen affinity, as suggested by Dujic *et al.* [14]; and elevated cerebral blood flow via hypercapnia-mediated increases in endogen catecholamines [34,35]. Investigating the prevalence of this phenomenon across divers, diving depths/durations and disciplines, as well as the underlying drivers of this phenomenon, is worthy of future, targeted investigation. Additionally, inclusion of control NIRS data from non-elite freedivers would be valuable in assessing underlying impacts of variability in individuals' physiology, function of elite conditioning or impact of factors such as NIRS probe placement. Nevertheless, dynamics such as changes in the contribution to the NIRS signal from [ΔHHb] close to the end of long dives, and in some cases dramatic TSI changes with changes in respiratory mechanics

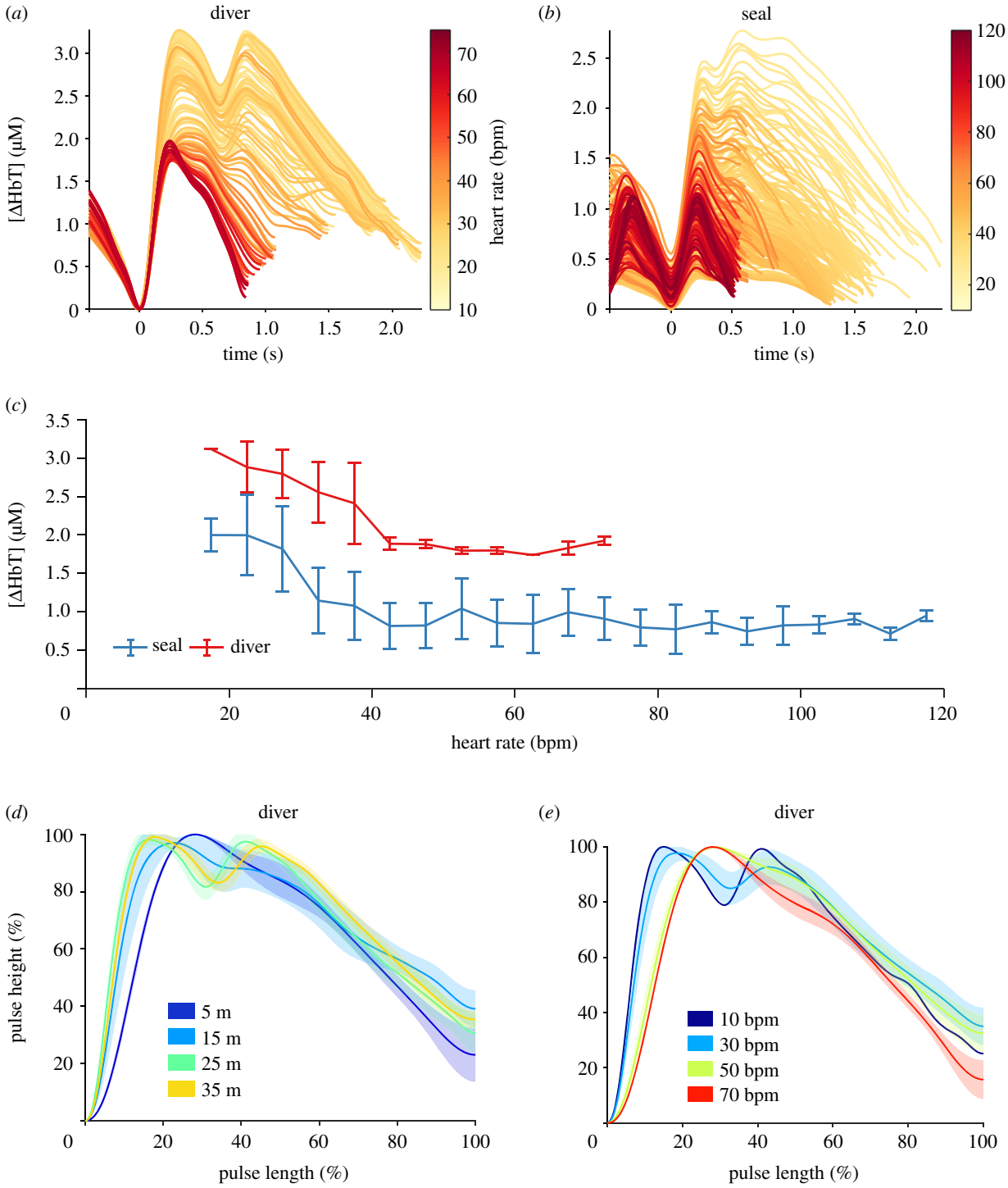

Figure 5. Cardiac pulsation of [ΔHbT] compared between a grey seal and human diver. The cardiac pulsation of [ΔHbT] for one example dive (*a*) is compared to the resting state cardiac pulsation in a grey seal (*b*). The colour encodes the underlying heart rate, revealing increasing pulse magnitude with bradycardia heart rate. (*c*) Comparing the human diver from (*a*) and the grey seal in (*b*), the average [ΔHbT] (sum of oxyhaemoglobin and deoxyhaemoglobin) magnitude, with errorbars spanning the standard deviation within the 5 bpm interval in heart rate, reveals similar trends. The pulse shape change in the human diver is emphasized by normalizing the pulses in length and height. Pulses are then averaged based on the underlying diving depth (*d*) and heart rate (*e*), with shaded error bars spanning the standard deviation of the normalized [ΔHbT] at any given time of the pulse. (Online version in colour.)

before diving, highlight additional information that CW-NIRS can provide alongside tissue-specific perfusion changes.

(b) Arterial oxygen saturation

Measurements of SpO_2 are not common in free-ranging animals, nor deep-diving humans, particularly those derived through optical measurement. The successful extraction here of SpO_2 from the NIRS signal, in combination with CBV and cerebral TSI changes, is an informative physiological combination—linking arterial blood oxygen delivery with tissue-specific blood oxygenation and haemodynamics changes, which could be particularly interesting when assessing cerebrovascular dynamics in breath-hold diving animals.

In all freedivers, SpO_2 remained high throughout the descent phase of each dive. Elevated ambient pressure associated with descent and resultant elevated alveolar and arterial pO_2 serve to maintain SpO_2 close to levels at the onset of the dive.

Shortly after the start of the ascent phase of each dive, SpO_2 began to decline and continued to do so throughout the remainder of the dive. As ambient pressure declines during ascent, alveolar and arterial PO_2 decline causing the reduction in SpO_2. Elevated heart rate during early ascent, reflecting the enhanced exertion when the diver swims up against negative buoyancy, increases cardiac output, which may also affect the decline of SpO_2 [11]. As such, reperfusion of previously ischaemic body compartments elevating whole-body oxygen consumption rate, along with depth-specific reduction in blood oxygen tension and/or exercise-induced stimulation tachycardia [3], could also explain why the rate of decline in SpO_2 increased throughout ascent (figures 2 and 3*a*). Interestingly, end-dive SpO_2 values on longer dives were at times below those experienced by humans climbing Mount Everest [36], with the lowest SpO_2 value recorded in the current study at 25% (figure 3*a*)—a value normally not compatible with consciousness [7]. It should also be noted that owing to the FFT window size in the SpO_2 extraction process, the desaturation to 25% SpO_2 was potentially exceeded before surfacing. This confirms that freedivers are at risk of syncope during ascent, in line with the concept of 'shallow water blackout' [18].

(c) Cardiac responses

As heart rate has been measured in several marine mammals and with application in energetics assessments [37], a capacity to relate cardiac changes to arterial oxygenation and tissue-specific haemodynamic and oxygenation changes via NIRS, could be useful for both comparative physiological comparison and energetic measurements.

The overall patterns of change in heart rate in the freedivers were similar to those previously reported for elite deep-freediving humans [38] and small/medium-sized marine mammals [32] (figure 3). Following the onset of diving, heart rate dropped until the bottom of the dive (figures 2 and 3*b*). Elicitation of the diving response upon diving by apnoea and stimulation of peripheral facial receptors [3] results in bradycardia which maintains arterial blood pressure during selective peripheral constriction, supporting the downregulation of oxygen consumption [2]. Minimum heart rates were reached at the bottom of the dive after a period of passive descent during 'free fall' before showing an overall increase during ascent involving exercise (figures 2 and 3*b*). The inverse relationship between heart rate and depth supports the assumption that beyond regulation of heart rate by the diving response, changes in intrathoracic pressure and lung volume may also influence heart rate via a change in activity from pulmonary stretch receptors in humans [39] just as in diving mammals [32]. The overall patterns of change in heart rate in human freedivers and sea lions, for instance, are strikingly similar (figure 3*b*).

The magnitude of reduction in heart rate exhibited by the freedivers was pronounced (figure 2) which is in accordance with earlier reports [40]. As shown in figure 4*a* (red line), where a diver exhibits less than 27 beats over 60 s, sustained exceptionally low heart rates were not uncommon and consistent with previous studies of apnoeic cardiovascular responses [41].

Progressive changes in cardiac waveforms with heart rate and depth—specifically, the increased height of the percussive peak (pulse magnitude) and the increased prominence of the tidal peak (figure 4*c*) at lower heart rates, were consistent with development of bisfirens pulse. Elevated pulse magnitude is indicative of increased blood flow [23] that can be associated with phenomena such as high arterial pressure [42] and changes in vascular compliance [43]. The prominence of a tidal wave is related to longer and slower systole owing to high arterial pressure with reduced stroke volume. This is apparent in the relationship between elevated pulse height and tidal peak prominence and heart rate—specifically at low heart rates (figure 5*c*). Low heart rates displayed by the freedivers are indicative of pronounced arterial restriction. Normally, central elastic arteries act to expand and recoil effectively within each cardiac cycle, providing a Windkessel effect to dampen haemodynamic pulsatility and facilitate a continuous blood flow in the capillaries [44]. However, we speculate that the level of arterial restriction and compliance loss at low heart rates less than 40 bpm may lead to a less effective Windkessel function, enhancing the high flow, low resistance cerebral pulsatility, thereby generating an increase in percussive peak in the cardiac waveform.

Additional information that can be garnered through appropriate signal analysis of NIRS data, as demonstrated here for the human data and transferred to a seal (figure 5), could provide insights or open new questions into comparative cardiovascular performance of diving mammals.

5. Conclusion

Overall, this study demonstrates the ability of CW-NIRS to provide non-invasive and continuous measurement of the patterns of cerebral oxygenation, haemodynamics and cardiac responses of freedivers conducting deep dives. In humans, NIRS has the potential to be an important tool to improve divers safety. Further, elite human freedivers could act as a tractable diving model as the continuous and high-quality NIRS signal recorded by a single wearable system, served as a proof of principle of CW-NIRS as a physiological measurement tool in a challenging environment. Transferability of signal processing methods, demonstrated here between human diver and seal data, highlights that the NIRS has broader application than only humans, and could begin to help fill knowledge gaps in the diving physiology of free-ranging animals.

Ethics. Scientific procedures involving freedivers complied with the Helsinki agreement and were approved by the Regional Committee for Medical and Health Research Ethics (Dnr 2019-05147). Procedures for capture, handling and housing of animals conformed to the Animals (Scientific Procedures) Act 1986, under the Sea Mammal Research Unit's Home Office licence (no. 70/7806) and were performed by personnel deemed competent under EU directive of the protection of animals used for scientific purposes.

Data accessibility. All seal data and all code are available at 10.6084/m9.figshare.14207864. Human data cannot be provided owing to conflict with ethical approval and potential breaches in anonymity owing to the exceptional diving depths and durations reached.

Authors' contributions. J.C.M.: conceptualization, methodology, software, formal analysis, investigation, data curation, writing, visualization. E.M.: investigation, writing—review and editing, project administration. A.R.: software, formal analysis, investigation, visualization, writing. J.K.: conceptualization, methodology, software, writing. N.H.: software, writing—original draft. J.W.: software, formal analysis, writing original draft. S.B.: methodology, resources, writing—review and editing. M.B.: methodology, resources, writing. J.M.H.: software, formal analysis, resources and writing—review and

editing. F.P.: data interpretation and writing. K.S.: resources and writing—review and editing. G.D.H.: resources, writing—review and editing, and funding acquisition (seal data). P.T.: resources and writing—original draft. E.S.: conceptualization, resources and contacts, data interpretation and writing, project administration and funding acquisition (human data).

Competing interests. We declare we have no competing interests.

Funding. Funding for human data was obtained through a donation from the Francis family, to the Swedish Centre for Research in Sports and Mid-Sweden University, in memory of their son/brother, who drowned from hypoxic blackout while snorkeling and holding his breath to dive underwater. Grey seal NIRS data were funded as part of the Department for Business, Energy and Industrial Strategy Offshore Energy Strategic Environmental Assessment programme. Supplementary funding supporting J.K. and A.R. was provided by US Office of Naval Research (ONR) grant no. N00014-19-1-1223.

Acknowledgements. We thank the elite freedivers for their kind cooperation, and Mr Marick Le Hérissé for help to carry out this study. We thank Mr Sean McHugh and Mr Philippe Hubert for assistance in the construction of the PortaDiver and Mr Simon Moss and Mr Ryan Milne for their roles in performing animal experiments.

References

1. Scholander PF. 1940 Experimental investigations on the respiratory function in diving birds and mammals. *Hvaldradets Skr.* **22**, 1–31.
2. Andersson J, Schagatay E. 1998 Arterial oxygen desaturation during apnea in humans. *Undersea Hyperbar. Med.* **25**, 21–25.
3. Daly M. 2011 Interactions between respiration and circulation. In *Handbook of physiology: the respiratory system II* (eds NS Cherhiack, JG Widdicombe), pp. 529–594. Bethesda, MD: American Physiology Society.
4. Blix AS, Elsner R, Kjekshus JK. 1983 Cardiac output and its distribution through capillaries and A-V shunts in diving seals. *Acta Physiol. Scand.* **119**, 109–116. (doi:10.1111/j.1748-1716.1983.tb07250.x)
5. Blix AS, Folkow B. 1983 Cardiovascular adjustments to diving in mammals and birds. In *Handbook of physiology. The cardiovascular system. Peripheral circulation and organ blood flow* (eds DM Casson, K Ronald), pp. 917–945. Bethesda, MD: American Physiology Society.
6. Kooyman GL, Wahrenbrock EA, Castellini MA, Davis RW, Sinnett EE. 1980 Aerobic and anaerobic metabolism during voluntary diving in Weddell seals: evidence of preferred pathways from blood chemistry and behavior. *J. Comp. Physiol.* **138**, 335–346. (doi:10.1007/BF00691568)
7. Schagatay E. 2011 Review: Predicting performance in competitive apnea diving. Part III: depth. *Diving Hyperbar. Med.* **41**, 216–228.
8. Meir JU, Champagne CD, Costa DP, Williams CL, Ponganis PJ. 2009 Extreme hypoxemic tolerance and blood oxygen depletion in diving elephant seals. *Am. J. Physiol.* **297**, 927–939. (doi:10.1152/ajpregu.00247.2009)
9. McDonald BI, Ponganis PJ. 2013 Insights from venous oxygen profiles: oxygen utilization and management in diving California sea lions. *J. Exp. Biol.* **216**, 3332–3341. (doi:10.1242/jeb.085985)
10. Bosco G, Rizzato A, Martani L, Schiavo S, Talamonti E, Garetto G, Paganini M, Camporesi EM, Moon RE. 2018 Arterial blood gas analysis in breath-hold divers at depth. *Front. Physiol.* **9**, 1558. (doi:10.3389/fphys.2018.01558)
11. Qvist J *et al.* 1993 Arterial blood gas tensions during breath-hold diving in the Korean ama. *J. Appl. Physiol.* **75**, 285–293. (doi:10.1152/jappl.1993.75.1.285)
12. Zapol WM, Liggins GC, Schneider RC, Qvist J, Snider MT, Creasy RK, Hochachka PW. 1979 Regional blood flow during simulated diving in the conscious Weddell seal. *J. Appl. Physiol.* **47**, 968–973. (doi:10.1152/jappl.1979.47.5.968)
13. Davis RD, Kanatous SB. 1999 Convective oxygen transport and tissue oxygen consumption in Weddell seals during aerobic dives. *J. Exp. Biol.* **202**, 1091–1113. (doi:10.1242/jeb.202.9.1091)
14. Dujic Z, Uglesic L, Breskovic T, Valic Z, Heusser K, Marinovic J, Ljubkovic M, Palanda I. 2009 Involuntary breathing movements improve cerebral oxygenation during apnea struggle phase in elite divers. *J. Appl. Physiol.* **107**, 1840–1846. (doi:10.1152/japplphysiol.00334.2009)
15. Williams CL, Meir JU, Ponganis PJ. 2011 What triggers the aerobic dive limit? Patterns of muscle oxygen depletion during divers of emperor penguins. *J. Exp. Biol.* **214**, 1782–1812. (doi:10.1242/jeb.052233)
16. Fujimoto K, Sano Y. 2014 Applicability of near-infrared spectroscopy for measuring hemodynamics during breath-hold diving. *Jpn. J. Marit. Activ.* **3**, 24–29.
17. Williams T, Blackwell SB, Richter B, Sinding M-HS, Heide-Jorgensen MP. 2017 Paradoxical escape responses by narwhals (*Monodon monoceros*). *Science* **385**, 1328–1331. (doi:10.1126/science.aao2740)
18. Fitz-Clarke JR. 2018 Breath-hold diving. *Compr. Physiol.* **8**, 585–630. (doi:10.1002/cphy.c160008)
19. Ferrari M, Quaresima V. 2012 A brief review on the history of human functional near-infrared spectroscopy (fNIRS) development and fields of application. *Neuroimage* **63**, 921–935. (doi:10.1016/j.neuroimage.2012.03.049)
20. McKnight JC *et al.* 2019 Shining new light on mammalian diving physiology using wearable near-infrared spectroscopy. *PLoS Biol.* **17**, e3000306. (doi:10.1371/journal.pbio.3000306)
21. Tisdall MM, Taylor C, Tachtsidis I, Leung TS, Pritchard C, Elwell CE, Smith M. 2009 The effect on cerebral tissue oxygenation index changes in the concentrations of inspired oxygen and end-tidal carbon dioxide in healthy adult volunteers. *Anesth. Analg.* **109**, 906–913. (doi:10.1213/ane.0b013e3181aedcdc)
22. Menssen J, Colier W, Hopman J, Liem D, de Korte C. 2009 A method to calculate arterial and venous saturation from near-infrared spectroscopy. *Adv. Exp. Med. Biol.* **645**, 135–140. (doi:10.1007/978-0-387-85998-9_21)
23. Elgendi M. 2012 On the analysis of fingertip photoplethysmogram signals. *Curr. Cardiol. Rev.* **8**, 14–25. (doi:10.2174/157340312801215782)
24. Sassaroli A, Fantini S. 2004 Comment on the modified Beer-Lambert law for scattering media. *Phys. Med. Biol.* **49**, N255–N257. (doi:10.1088/0031-9155/49/14/N07)
25. Suzuki S, Takasaki S, Ozaki T, Kobayashi Y. 1999 A tissue oxygenation monitor using NIR spatially resolved spectroscopy. *Proc. SPIE* **3597**, 582–592. (doi:10.1117/12.356862)
26. Al-Rawi PG, Smielewski P, Kirkpatrick PJ. 2001 Evaluation of a near-infrared spectrometer for detection of intracranial oxygenation changes in the adult head. *Stroke* **32**, 2492–2500. (doi:10.1161/hs1101.098356)
27. Örnhagen HE, Schagatay E, Andersson J, Bergsten E, Gustafsson P, Sandstrom S. 1998 Mechanisms of 'buccal pumping'. Manuscripts for the XXIV annual scientific meeting of the European Underwater and Baromedical Society 1998, Stockholm, Sweden, 12–15 August, pp. 80–83.
28. Hakimi N, Setarehdan SK. 2018 Stress assessment by means of heart rate derived from functional near-infrared spectroscopy. *J. Biomed. Opt.* **23**, 1. (doi:10.1117/1.jbo.23.11.115001)
29. Scholkmann F, Boss J, Wolf M. 2012 An efficient algorithm for automatic peak detection in noisy periodic and quasi-periodic signals. *Algorithms* **5**, 588–603. (doi:10.3390/a5040588)
30. Leung TS, Tachtsidis I, Velayuthan P, Oliver C, Henty JR, Jones H, Smith M, Elwell CE, Delpy ST. 2006 Investigation of oxygen saturation derived from cardiac pulsations measured on the adult head using NIR spectroscopy. In *Oxygen transport to tissue XXVII. Advances in experimental medicine and biology*, vol. 578 (eds G Cicco, DF Bruley, M Ferrari, DK Harrison), pp. 209–215. New York, NY: Springer.
31. Franceschini MA, Gratton E, Fantini S. 1999 Noninvasive optical method of measuring tissue and arterial saturation: an application to absolute pulse oximetry of the brain. *Opt. Lett.* **24**, 829–831. (doi:10.1364/OL.24.000829)

32. McDonald BI, Ponganis PJ. 2014 Deep-diving sea lions exhibit extreme bradycardia in long duration dives. *J. Exp. Biol.* **217**, 1525–1534. (doi:10.1242/jeb.098558)
33. Novalija J, Lindholm P, Loring SH, Diaz E, Fox JA, Ferrigno M. 2007 Cardiovascular aspects of glossopharyngeal insufflation and exsufflation. *Undersea Hyperb. Med.* **34**, 415–423.
34. Eichhorn L, Erdfelder F, Kessler F, Doerner J, Thudium MO, Meyer R, Ellerkmann RK. 2015 Evaluation of near-infrared spectroscopy under apnea-dependent hypoxia in humans. *J. Clin. Monit. Comput.* **29**, 749–757. (doi: 10.1007/s10877-015-9662-2.).
35. Eichhorn L *et al.* 2018 Cardiovascular magnetic resonance assessment of acute cardiovascular effects of voluntary apnoea in elite divers. *J. Cardiovasc. Magn. Reson.* **20**, 40. (doi: 10.1186/s12968-018-0455-x)
36. Grocott MPW, Martin DS, Levett DZH, McMorrow R, Windsor J, Montgomery H. 2009 Arterial blood gases and oxygen content in climbers on Mount Everest. *N. Engl. J. Med.* **360**, 140–149. (doi:10.1056/NEJMoa0801581)
37. Nolet BA, Butler PJ, Masman D, Woakes AJ. 1992 Estimation of daily energy expenditure from heart rate and doubly labelled water in exercising geese. *Physiol. Zool.* **65**, 1188–1216. (doi:10.1086/physzool.65.6.30158275)
38. Lemaître F, Lafay V, Taylor M, Costalat G, Gaedette B. 2013 Electrocardiographic aspects of deep diving in elite breath-hold divers. *Undersea Hyperb. Med.* **40**, 145–154.
39. Andersson J, Schagatay E. 1998*b* Effects of lung volume and involuntary breathing movements on the human diving response. *Eur. J. Appl. Physiol.* **77**, 19–24. (doi:10.1007/s004210050294)
40. Ferretti G. 2001 Extreme human breath-hold diving. *Eur. J. Appl. Physiol.* **84**, 254–271. (doi:10.1007/s004210000377)
41. Lindholm P, Sundblad P, Linnarsson D. 1999 Oxygen-conserving effects of apnea in exercising men. *J. Appl. Physiol.* **87**, 2122–2127. (doi:10.1152/jappl.1999.87.6.2122)
42. Xing X, Sun M. 2016 Optical blood pressure estimation with photoplethysmography and FFT-based neural networks. *Biomed. Opt. Express* **7**, 3007–3020. (doi:10.1364/BOE.7.003007)
43. O'Rourke MF, Nichols WW. 2005 Aortic diameter, aortic stiffness, and wave reflection increase with age and isolated systolic hypertension. *Hypertension* **45**, 652–658. (doi:10.1161/01.HYP.0000153793.84859.b8)
44. Nichols WW, O'Rourke MF. 2005 *Mcdonald's blood flow in arteries*. New York, NY: Oxford University Press.